Research paper

Burning characteristics of agglomerated aluminum particles in the reaction zone and the luminous flame of AP composite propellants

Rieko Doi*†, Takuo Kuwahara*, Kengo Yamamoto**, and Apollo B. Fukuchi**

*Department of Aerospace Engineering, College of Science and Technology, Nihon University
7-24-1, Narashino-dai, Funabashi, Chiba, 274-8501, JAPAN
Phone : +81-47-469-5317
†Corresponding author : csri11083@g.nihon-u.ac.jp

**IHI AEROSPACE Co., Ltd., 900, Fujiki, Tomioka, Gunma 370-2398, JAPAN

Received : November 21, 2014 Accepted : October 9, 2015

Abstract

Aluminum (Al) particles as a metal fuel are easy to agglomerate at the burning surface of composite propellants. The diameters of the agglomerated Al particles are larger than that of the initial Al particle. It is known that the luminous flames are nearly spherical in shape at the average diameter of the luminous flames. The heterogeneity of the gas phase influences the distance from the luminous flames to the agglomerated Al particles in the lateral direction of the plane surface. The gas phase composition influences the intensity of the brightness of the luminous flames.

Keywords : luminous flame, brightness, mole fraction, aluminum particle, agglomeration

1. Introduction

It is known that aluminum (Al) particles easily agglomerate at the burning surface of composite propellants in solid rockets[1]. The agglomerated Al particle diameter becomes larger than the diameter of the Al powders mixed in the propellant[2]. The burning time of agglomerated Al particles increases with increasing the diameter. The data scatter of the burning time is readily apparent even when they have the same Al particle diameter. The combustion efficiency of the propellants decreases because the burning time of agglomerated Al particles increases[3].

It is known that the solid phase of composite propellants is heterogeneous. The gas phase heterogeneity of the reaction zone is influenced by the heterogeneity in the composite propellants[4),5]. When the agglomerated Al particles ignite, the luminous flame appears around the agglomerated Al particles[6)-16]. Since the agglomerated Al particle diameter is small, the temperature of the agglomerated Al particles is uniform. When the burning rate of the agglomerated Al particles is uniform, the shape of the luminous flame is nearly spherical around the agglomerated Al particles. The shape of the luminous flame is influenced by the flow condition in the gas phase. In turn, the flow condition is influenced by the gas phase. However, it has not been clarified the influences of the heterogeneity of the gas phase on the luminous flame of the agglomerated Al particles. In addition, it has not been clarified where the difference of the gas phase compositions influences the luminous flame of the agglomerated Al particles.

In this study, we broaden the reaction zone at 0.1 MPa. At 0.1 MPa pressure, the influences of the heterogeneity of the gas phase and the composition on the luminous flame of the agglomerated Al particles are magnified. This study evaluated the influences of the heterogeneity of the gas phase on the shape of the luminous flame and the influences of the difference of the gas phase composition on the luminous flame brightness. The results were obtained from the brightness of the luminous flame of the agglomerated Al particles in the reaction zone. We clarified that the heterogeneity of the gas phase influences the distance from the luminous flames to the agglomerated Al particles in the lateral direction of the

plane surface.

2. Theoretical analysis

The burning time depends on the square of the agglomerated Al particle diameter and the constant k. The data scatter of the burning time is readily apparent even when they have the same Al particle diameter. The relationship between the constant k and the luminous flame temperature T_f is obtained in the following steps. Symbols are described in the section Symbols. The law of the conservation of the energy exists in the reaction zone of the Al particles. The following equation indicates the evaporation energy per unit time Q_1.

$$Q_1 = \pi D_0^2 r_e \rho_{Al} L \tag{1}$$

The following equation indicates the heat transfer Q_2 from the luminous flame to the Al particle.

$$Q_2 = \pi D_0^2 h\,(T_f - T_s) \tag{2}$$

From the energy balance, Q_1 equals to Q_2 and the next equation is obtained.

$$\pi D_0^2 r_e \rho_{Al} L = \pi D_0^2 h\,(T_f - T_s) \tag{3}$$

The linear burning rate r_e is as follows.

$$r_e = \frac{1}{2}\frac{dD_0}{dt} \tag{4}$$

The liquid Al particle is a sphere and the burning time t_e is obtained using the following equation from the D_0^2 law[16].

$$t_e = kD_0^2 \tag{5}$$

From Equation (4) and the differentiated Equation (5), the linear burning rate is obtained.

$$r_e = \frac{1}{4kD_0} \tag{6}$$

To obtain the coefficient of the heat transfer, the Nusselt number Nu represents as the following equation.

$$Nu = \frac{hD_0}{\lambda} \tag{7}$$

Nu is 2 in this study because the Reynolds number R_e is too small. From Equations 3, 6, and 7, Equation 8 is obtained.

$$k = \frac{\rho_{Al} L}{8\lambda\,(T_f - T_s)} \tag{8}$$

In Equation 8, ρ_{Al} (2700 kg m^{-3}), L (10896 kJ kg^{-1}) of the Al particle, λ is the constant in this study. The surface temperature of the agglomerated Al particles is assumed by the boiling point and is the constant at the same pressure. Thus, we observed the luminous flame temperature with the luminous flame brightness.

3. Experiment

3.1 Composition of sample propellants

Compositions of three sample propellants are shown in Table 1. One of the sample propellants, the AN/Oct, consists of an ammonium perchlorate (AP) and an ammonium nitrate (AN) as oxidizers, an octadecyl alcohol (Oct : $C_{18}H_{38}O$) as a binder, and the Al powders as a metal fuel. The others sample propellants, the HTPB 1 and the HTPB 2, consist of AP as oxidizers, a hydroxyl-terminated polybutadiene (HTPB) as a binder, and the Al powders as a metal fuel. The mean AP particle diameters are 50 and 200 μm. The mean Al particle diameter is 30 μm. To observe the difference of the mole fraction, we use two types of the propellants, the HTPB 1 and the HTPB 2, at the concentrations of AP, 80 parts and 92.5 parts, respectively. These concentrations of AP have the major difference about the mole fraction for the HTPB 1 and the HTPB 2 propellants. We use the AN/Oct propellant with 80 AP parts. This concentration of AP has the major difference about the mole fraction for the AN/Oct and the HTPB 2 propellants. Table 2 shows the burning rates r of the propellants at 0.1 MPa. The value of the reaction zone thickness is about 1 mm[9]. The theoretical adiabatic flame temperature without Al of the AN/Oct propellant is 2314 K. The adiabatic flame temperature of the HTPB 1 propellant is 2868 K and of the HTPB 2 propellant is 2674 K[13]. The theoretical mole fractions are shown in Figures 1 and 2[13]. These figures show the changes of the mole fractions when the concentration of AP changes from 80 parts to 90 parts for the AN/Oct propellant, and from 80 parts to 92.5 parts for the HTPB propellant. In comparison, the AN/Oct and the HTPB 1 propellants have about two times as much mole fractions (H_2O, CO_2, O_2) as the HTPB 2 propellant.

Table 1 Compositions of three sample propellants.

Sample propellant	Composition [%]				
	AP	AN	Oct	HTPB	Al
AN/Oct	80	10	10	–	20
HTPB 1	92.5	–	–	7.5	20
HTPB 2	80	–	–	20	20

Table 2 Burning rates of three sample propellants.

Sample propellant	Burning rate r [mm s^{-1}]
AN/Oct	0.40
HTPB 1	0.89
HTPB 2	1.37

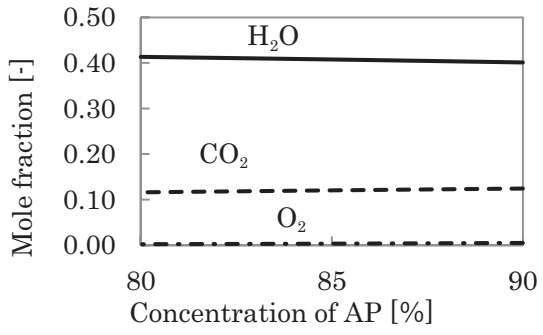

Figure 1 Relation between mole fraction and AP concentration for AN/Oct propellant.

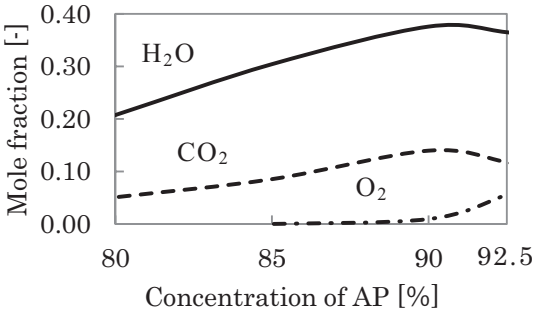

Figure 2 Relation between mole fraction and AP concentration for HTPB propellant.

3.2 Experimental method

An experimental apparatus is portrayed in Figure 3. The sample propellants burned at 0.1 MPa in the N_2 gas atmosphere. The burning surface images were taken with a microscope at the 40 magnifications attached to a high speed camera. The value of a field depth is about 1 mm. A sampling rate of the high speed camera is 8000 fps. A number of pixels of figures is 3315×3315. The gravitational force is directed downward in Figure 3. The sample propellant size is shown in Figure 4. The cylindrical sample propellant diameter is 10 mm.

3.3 Experimental analysis

The figures of the agglomerated Al particles and the luminous flames of the agglomerated Al particles are nearly spherical. The direction of the flow is as same as the direction of the tail of the luminous flame of the agglomerated Al particles. The agglomerated Al particle diameter was defined by observing the figure of the agglomerated Al particles, the brightness y, and the differentiated brightness $dy\ dx^{-1}$. In Figure 5, where D_0 is the agglomerated Al particle diameter, D_f is the luminous flame diameter, the x is the arbitrary length at the vertical direction of the flow and the flow direction is obtained by

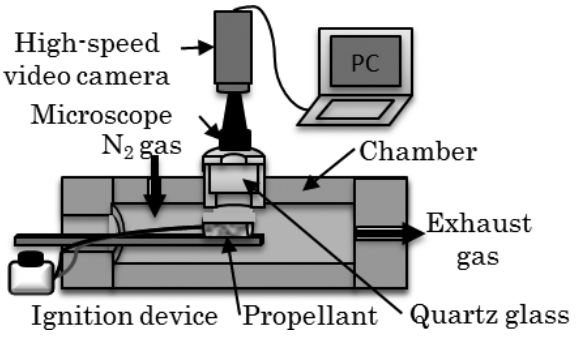

Figure 3 Experimental apparatus for observation of burning surface.

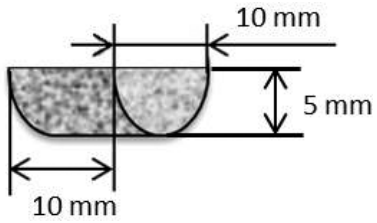

Figure 4 Sample propellant size.

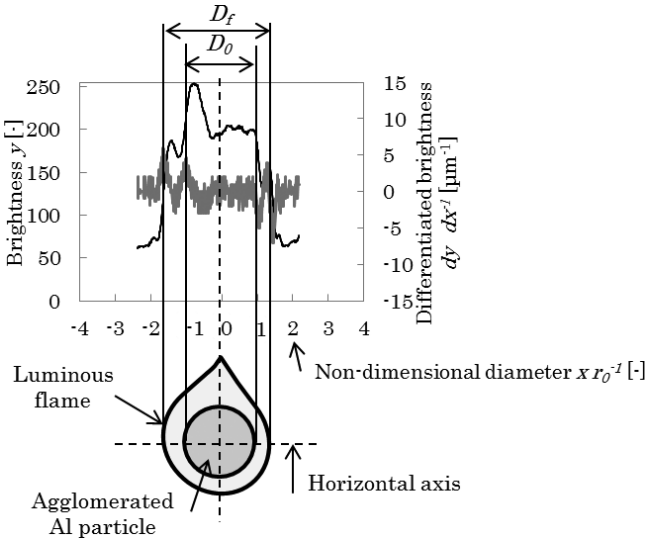

Figure 5 Experimental analysis.

the direction of the tail of the luminous flame of the agglomerated Al particles, and the dx is the differentiated x. We use the dx is 1 μm. The r_0 is the radius of the agglomerated Al particles. The r_0 equals D_0 divided by 2. The agglomerated Al particle diameter is measured to establish a basis for a non-dimensional diameter $x\ r_0^{-1}$. To observe the influence of the heterogeneity of the gas phase, we measure the brightness in the direction perpendicular to the flow rather than the other directions. Even as the luminous flame shape is an ellipse, the luminous flame in a direction perpendicular to the flow is the symmetrical shape. We defined the distance of the peaks of the differentiated brightness as the agglomerated Al particle diameter and the luminous flame diameter. The location of the inner peaks in the differentiated brightness is the same as the Al particle diameter and we defined the Al particle diameter in Figure 5. The non-dimensional diameter $x\ r_0^{-1}$ was divided into the two halves at the agglomerated Al particle center, as shown in Figure 5. The non-dimensional diameter of the agglomerated Al particles is −1 to 1.

We defined the agglomerated Al particle diameter and the luminous flame diameter as the following equations by the figure. The analysis method of the measurement is shown in Figure 6. The agglomerated Al particle diameter is measured at three directions and the agglomerated Al particle diameter is defined as the following Equation 9. The luminous flame diameter is defined same as the agglomerated Al particle diameter as the following Equation 10.

$$D_{0m} = \frac{(D_{01} + D_{02} + D_{03})}{3} \tag{9}$$

$$D_{fm} = \frac{(D_{f1} + D_{f2} + D_{f3})}{3} \tag{10}$$

4. Result and discussion

Figure 7 shows the agglomerated Al particles and the luminous flames in the reaction zone. In Figure 7, where

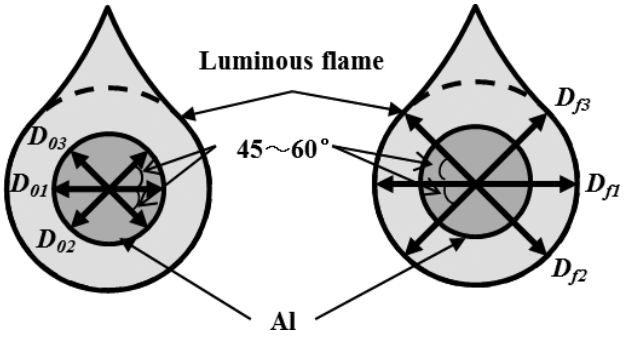

Figure 6 Analysis method of measurement.

D_{0m} is the average agglomerated Al particle diameter, D_{fm} is the average luminous flame diameter. We pick up almost the same agglomerated Al particle diameter in Figure 7 and these average agglomerated Al particle diameters and these average luminous flame diameters don't have dependence of the propellant composition. The agglomerated Al particles have a small cap and the Al jet is a really short time. The white broken line represents the burning surface of the propellant. We observed the agglomerated Al particles in the reaction zone of the propellants. Figures 8, 9 and 10 show the relation between the non-dimensional diameter $x\ r_0^{-1}$ and the brightness y, and between the $x\ r_0^{-1}$ and the differentiated brightness $dy\ dx^{-1}$. Figure 8 is shown for the AN/Oct propellant (Figure 7-①). Figures 9 (Figure 7-②) and 10 (Figure 7-③) are shown for the HTPB propellants.

The peak brightness of the luminous flame is located at the $x\ r_0^{-1} = -1.53$ on the left side of the agglomerated Al particles and the $x\ r_0^{-1} = 1.39$ on the right side of the Al particle in Figure 8. The ratio of the left side $x\ r_0^{-1}$ to the right side $x\ r_0^{-1}$ is 1.10 and it is larger than 1. The peak brightness of the luminous flame is located at the $x\ r_0^{-1} = -1.56$ on the left side of the agglomerated Al particles and the $x\ r_0^{-1} = 1.59$ on the right side of the agglomerated Al particles in Figure 9. The ratio of the left side $x\ r_0^{-1}$ to the right side $x\ r_0^{-1}$ is 0.98 and smaller than 1.

One of the ratios of the left ($x\ r_0^{-1}$) to the right ($x\ r_0^{-1}$) is over 1. The other of the ratios of the left ($x\ r_0^{-1}$) to the right ($x\ r_0^{-1}$) is under 1. One of the luminous flames moves just a little to the left, like as shown in Figures 7-① and 8. The other luminous flames move just a little to the right, like as shown in Figures 7-②and 9. It is considered that the heterogeneity of the gas phase influences the distance from the luminous flame to the agglomerated Al particles in the lateral direction of the plane surface. Since the burning rate of the agglomerated Al particles is the uniform, it is considered that the shape of the luminous flame is nearly spherical around the agglomerated Al particles. However, the luminous flame is influenced by the flow condition.

The brightness of the luminous flame for the AN/Oct and the HTPB 1 propellants are higher than that of the luminous flame for the HTPB 2 propellant. In Figure 8 for the AN/Oct propellant, the peaks of the differentiated brightness and the luminous flame are obvious at the agglomerated Al particle diameter and the luminous flame diameter. In Figure 9 for the HTPB 1 propellant, the peaks

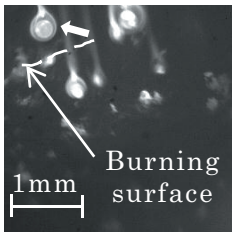

D_{0m}: 251[μm]
D_{fm}: 388[μm]
①AN/Oct

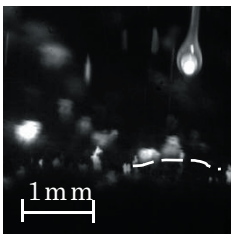

D_{0m}: 243 [μm]
D_{fm}: 372 [μm]
②HTPB 1

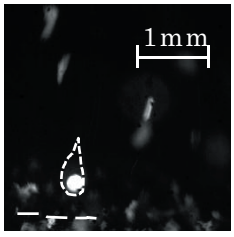

D_{0m}: 231 [μm]
D_{fm}: 329 [μm]
③HTPB 2

Figure 7 Formation of luminous flames.

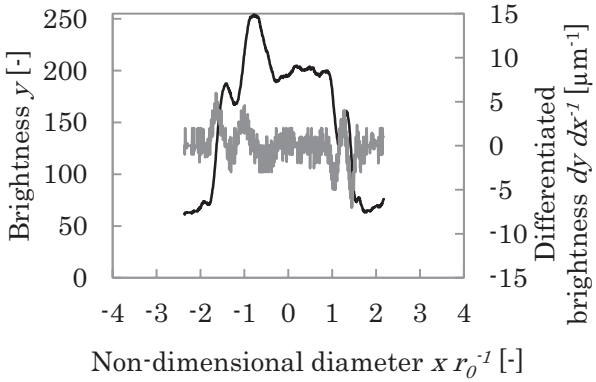

Figure 8 Relation between the y and $x\ r_0^{-1}$ in AN/Oct propellant (as shown in Figure 7-①).

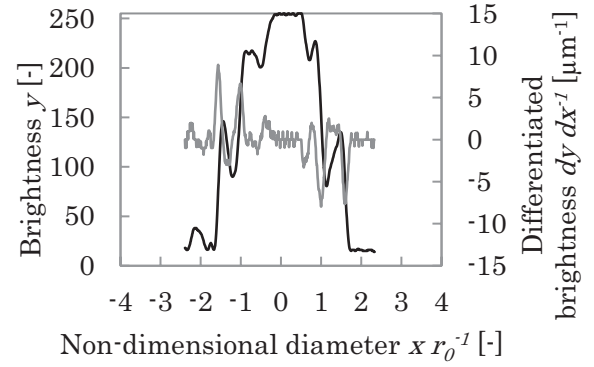

Figure 9 Relation between the y and $x\ r_0^{-1}$ in HTPB 1 propellant (as shown in Figure 7-②).

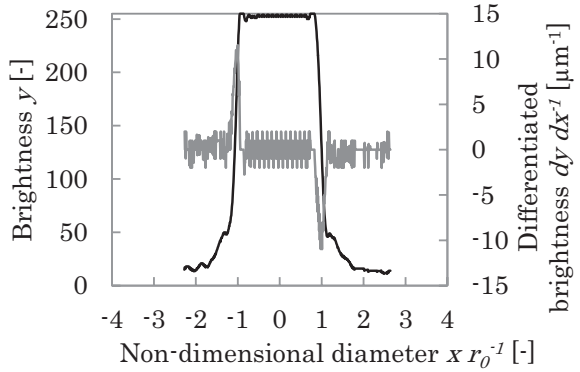

Figure10 Relation between the y and $x\ r_0^{-1}$ in HTPB 2 propellant (as shown in Figure 7-③).

of the differentiated brightness and the luminous flame are obvious. In Figure 10 for the HTPB 2 propellant, the peaks of the differentiated brightness appear faintly at the luminous flame diameter. It is considered that the difference of the brightness for the luminous flame between the propellants depends on the difference of the mole fractions of H_2O, CO_2, and O_2 around the agglomerated Al particles.

5. Conclusion

- The heterogeneity of the gas phase influences the distance from the luminous flame to the agglomerated Al particles in the lateral direction of the plane surface.
- The gas phase composition influences the intensity of the brightness of the luminous flame.

Symbols

D_0 − Agglomerated Al particle diameter / [m].
D_f − Luminous flame diameter of the agglomerated Al particle / [m].
h − Heat transfer coefficient / [$Wm^{-2}K^{-1}$].
L − Heat of the vaporization / [$kJkg^{-1}$].
Nu − Nusselt number / [-].
Q_1 − Evaporation energy per unit time / [W].
Q_2 − Heat transfer / [W].
R_e − Reynolds number / [-].
r − Burning rate of the propellant / [mms^{-1}].
r_e − Evaporation rate / [ms^{-1}].
T_f − Luminous flame temperature surrounding the Al particle / [K].
T_s − Surface temperature of the agglomerated Al particle / [K].
t_e − Burning time / [s].
ρ_{Al} − Al particle density / [kgm^{-3}].
λ − Heat conductivity / [$Wm^{-1}K^{-1}$].
k − Constant / [sm^{-2}].

Acknowledgment

This work was sponsored by the Foundation for the Promotion of the Industrial Explosives Technology.

Reference

1) N. S. Cohen, AIAA Journal, 21, 720−725 (1983).
2) H. Habu, Journal of Japan Institute of Light Metals, 58, 162−166 (2008) (in Japanese).
3) M. W. Beckstead, RTO/VKI Special Course on Internal Aerodynamics in Solid Rocket Propulsion, RTO−EN−023 (2004).
4) Propellant committee, "Propellant Handbook", Japan Explosives Society, 142, 245 (2005).
5) N. Kubota, "Propellants and Explosives : Thermochemical Aspects of Combustion, Second Rev. Exp.", Wiley− VCH, Verlag GmbH & Co. KGaA, 186−188 (2007).
6) T. Kuwahara, S. Sakai, R. Doi, T. Sasaki, and K. Takahashi, Proceedings of Autumn Meeting of Japan Explosives Society, 9 (2013) (in Japanese).
7) T. Sasaki, S. Sakai, R. Doi, K. Takahashi, and T. Kuwahara, 9 th International High Energy Materials, 1−5 (2013).
8) K. Takahashi, S. Oide, and T. Kuwahara, Propellant, Explosive, Pyrotechnics, 38, 555−562 (2013).
9) K. Takahashi, doctoral dissertation, Nihon University (2013) (in Japanese).
10) J. C. Melcher, H. Krier, and R. L. Burton, Journal of Propulsion and Power, 18, 631−640 (2002).
11) S. Oide, K. Takahashi, and T. Kuwahara, 48th AIAA/ASME/SAE/ASEE Joint Propulsion Conference, AIAA Paper, 2012−3973 (2012).
12) S. Oide, Master Thesis in Department of Aerospace Engineering, College of Science and Technology, Nihon University (2013) (in Japanese).
13) S. Gordon and B. J. McBride, "Computer program for calculation of complex chemical equilibrium compositions and applications", NASA Reference Publication, NASARP−1311 (1994).
14) L. T. DeLuca, L. Galfetti, F. Maggi, G. Colombo, A. Bandera, S. Cerri, and P. Donega, 2nd International Symposium on Propulsion for Space Transportation, ESA Space Propulsion, 1−10 (2008).
15) K. Kuo and M. Summerfield, "Fundamentals of solid propellant combustion", Prog. Astronaut. Aeronaut., 90, 479−514 (1984).
16) J. C. Melcher, J. T. Brzozowski, H. Krier, and R. L. Burton, 36 th AIAA / ASME / SAE / ASEE Joint Propulsion Conference and Exhibit, AIAA Paper, 2000−3333 (2000).